Nanoporous TiO_2 and WO_3 Films by Anodization of Titanium and Tungsten Substrates: Influence of Process Variables on Morphology and Photoelectrochemical Response†

N. R. de Tacconi,* C. R. Chenthamarakshan, G. Yogeeswaran,‡ A. Watcharenwong,§ R. S. de Zoysa, N. A. Basit,|| and K. Rajeshwar*

Center for Renewable Energy Science and Technology (CREST), The University of Texas at Arlington (UTA), Arlington, Texas 76019-0065

Received: July 17, 2006; In Final Form: August 31, 2006

The photoelectrochemical response of nanoporous films, obtained by anodization of Ti and W substrates in a variety of corrosive media and at preselected voltages in the range from 10 to 60 V, was studied. The as-deposited films were subjected to thermal anneal and characterized by scanning electron microscopy and X-ray diffraction. Along with the anodization media developed by previous authors, the effect of poly(ethylene glycol) (PEG 400) or D-mannitol as a modifier to the NH_4F electrolyte and glycerol addition to the oxalic acid electrolyte was studied for TiO_2 and WO_3, respectively. In general, intermediate anodization voltages and film growth times yielded excellent-quality photoelectrochemical response for both TiO_2 and WO_3 as assessed by linear-sweep photovoltammetry and photoaction spectra. The photooxidation of water and formate species was used as reaction probes to assess the photoresponse quality of the nanoporous oxide semiconductor films. In the presence of formate as an electron donor, the incident photon to electron conversion efficiency (IPCE) ranged from ∼130% to ∼200% for both TiO_2 and WO_3 depending on the film preparation protocol. The best photoactive films were obtained from poly(ethylene glycol) (PEG 400) containing NH_4F for TiO_2 and from aqueous NaF for WO_3.

Introduction

The photoelectrochemical behavior of semiconductor/electrolyte interfaces has been extensively studied for more than three decades, much of this interest being driven by solar energy conversion applications. Reviews of this early body of work exist.[1−4] On the other hand, corresponding studies on nanostructured semiconductor surfaces in contact with electrolytes have a more recent history.[5−8] Since the discovery of self-organized nanoporous structures on aluminum[9−12] and silicon,[13,14] it has been recently shown that anodization of Ti[15−28] or W[29,30] substrates in certain (corrosive) media also affords oxide semiconductor surfaces with interesting morphologies on the nanometer size scale. The photoelectrochemical aspects of these materials, however, have not been extensively studied, and this is especially true for WO_3. This then constitutes the focus of the present study; in particular, we describe below how changes in the anodization conditions and substrate surface history (e.g., surface treatment, electrolyte composition and additives, anodization voltage and time) influence the photoelectrochemical response of the resultant TiO_2 and WO_3 semiconductor surfaces. Further, we present the influence of two new modifiers in the anodization medium, namely, D-mannitol and poly(ethylene glycol), on the morphology of TiO_2 films and their photoelectrochemical response. An extensive set of experiments, both probing the nanopore morphology and the photoelectrochemical response, was performed for WO_3 because of the relative paucity of information[29,30] on this material.

Experimental Section

Chemicals and Materials. All chemicals were from commercial sources and the highest purity available. Deionized water (18 MΩ cm) was used in all cases for making solutions. D-Mannitol (Alfa Aesar, 99%) and poly(ethylene glycol) (M_n ca. 400, Aldrich) were used as received. Either titanium foil (Alfa Aesar, 0.25 mm thick, 99.95%) or tungsten foil (Alfa Aesar, 0.25 mm thick, 99.95%) was used as the substrate for growth of nanoporous oxide films. Strips (1.4 cm × 1.4 cm) were cut and mechanically polished to mirror finish using silicon carbide sandpaper of successively finer roughness (220, 320, 600, 1200, 1500, and 2000 grit) followed by alumina micropolish suspension down to 0.05 μm. They were then cleaned in three 5 min steps in ultrasonicated acetone, 2-propanol, and finally ultrapure water and then dried in flowing N_2 stream and used immediately.

Electrosynthesis. Nanostructured TiO_2 and WO_3 films were grown by anodization of titanium and tungsten foils, respectively. The anodization was performed in a two-electrode electrochemical cell and in different electrolyte media (see Table 1) using a large platinum coil as a cathode. The oxide films were grown using preselected anodization voltages in the range from 10 to 60 V. Anodization employed a multioutput power supply (Switching System International, CA) or a 420X Power Supply (The Electrosynthesis Company, Inc., NY). The electrochemical cell was connected in series to a variable resistor (100 kΩ) that was decreased to zero to simulate a voltage ramp of ∼0.2 V/s, and then the voltage was held at the preselected level for anodization times varying from 1 to 10 h. The metal

† Part of the special issue "Arthur J. Nozik Festschrift".

* To whom correspondence should be sent. E-mail: N. R. de Tacconi, ntacconi@uta.edu; K. Rajeshwar, rajeshwar@uta.edu.

‡ Materials Science and Engineering Program, UTA.

§ National Research Center for Environmental and Hazardous Waste Management, Chulalongkorn University, Bangkok, Thailand.

|| Nanofab Center, UTA.

10.1021/jp064527v CCC: $33.50
Published on Web 10/12/2006

TABLE 1: Anodization Conditions, Photoelectrochemical Performance, and Morphology of Nanoporous Films on Ti and W Substrates in This Study

entry no.	metal substrate	electrolyte, medium modifier	anodization voltage, time	j_{ph}^{W}/mA cm^{-2} [a]	j_{ph}^{F}/mA cm^{-2} [b]	morphology[c]
1	Ti	0.15 M NH_4F/glycerol	15 V, 10 h	3.05	5.01	nanoporous
2			20 V, 5 h	2.11	5.45	S-O[d] nanotubes, 40 nm[e]
3			20 V, 10 h	3.41	5.57	S-O nanotubes, 40 nm
4			35 V, 10 h	2.31	3.77	S-O nanotubes, 89 nm
5			40 V, 10 h	n.d.[f]	n.d.	S-O nanotubes, 89 nm
6			55 V, 10 h	1.28	2.00	disordered nanotubes
7	Ti	0.15 M NH_4F glycerol:H_2O (90:10)	20 V, 5 h	1.25	n.d.	S-O nanotubes, 40 nm
8		PEG 400:H_2O (90:10)	20 V, 5 h	2.54	n.d.	S-O nanotubes, 108 nm
9		1.4 M D-mannitol	20 V, 5 h	2.16	n.d.	S-O nanotubes, 140 nm
10	W	0.15 NH_4F/glycerol	20 V, 5 h	1.51	1.02	nanoholes, 13 nm
11			20 V, 10 h	2.06	4.42	nanoholes, 13 nm
12			35 V, 5 h	2.82	3.79	nanoholes, 25 nm
13	W	0.30 M oxalic acid	10 V, 1 h	0.90	n.d.	nanocubes
14			35 V, 30 min	n.d.	n.d.	nanobowls, 44-85 nm
15			35 V, 1h	2.90	4.63	nanobowls, 44-85 nm
16			55 V, 1 h	1.08	2.71	collapsed nanowires
17			55 V, 5 h	1.47	3.75	collapsed nanowires
18			60 V, 1 h	n.d.	n.d.	collapsed nanowires
19	W	0.30 M oxalic acid glycerol: H_2O (25:75)	35 V, 1 h	2.82	4.64	many nanobowls
20		glycerol: H_2O (75:25)	35 V, 1 h	1.57	2.67	few nanobowls
21		glycerol: H_2O (90:10)	35 V, 2 h	1.75	2.92	very few nanobowls
22		glycerol: H_2O (90:10)	55 V, 4 h	1.78	3.12	smooth film
23	W	0.15 M NaF	60 V, 1 h	0.63	1.02	nanoporous
24			60 V, 3 h	3.52	5.42	nanoporous
25			60 V, 6 h	2.02	3.79	nanoporous
26	W	0.15 M NaF, 0.05 M HF	60 V, 1 h	0.47	0.73	nanoporous

[a] j_{ph}^{W} = photocurrent density in 0.5 M Na_2SO_4 at 1.4 and 2.0 V for TiO_2 and WO_3, respectively. [b] j_{ph}^{F} = photocurrent density in 0.5 M Na_2SO_4 + 0.1 M HCOONa at 1.5 and 2.0 V for TiO_2 and WO_3, respectively. [c] As assessed by SEM. [d] S-O = self-organized. [e] Nanopore diameter. [f] No data.

foil (either Ti or W) was pressed between a set of O rings in the electrochemical cell, leaving 0.61 cm^2 exposed to the electrolyte, and the electric contact was located on the backside of the sample. Once the oxide films were grown, the anodized metal foils were removed from the O-ring assembly and carefully washed by immersion in deionized water and then dried in a N_2 stream.

Photoelectrochemistry. A standard single-compartment, three-electrode electrochemical cell was used for the photoelectrochemical measurements. A large Pt coil and an Ag|AgCl|satd. KCl reference electrode (Microelectrode Inc., NH), along with the working electrode, completed the cell setup. All potentials in the photoelectrochemical data below are quoted with respect to this reference electrode. The UV light source was a 150 W xenon arc lamp (Oriel, Stratford, CT). The nominal incident photon flux at the location of the photoelectrode was 0.59 mW/cm^2 at 340 nm with a bandwidth of 4 nm. The photon flux was monochromatically measured on an Oriel model 70260 Radiant Power/Energy meter, and the flux quoted above is not corrected for reflection losses by cell windows, etc. The radiation source was placed 8 cm away from the working electrode surface. Photovoltammetry profiles were recorded on a model CV-27 Voltammograph (Bioanalytical Systems, West Lafayette, IN) equipped with a model VP-6414S Soltec X−Y recorder in 0.5 M Na_2SO_4 electrolyte without and with 0.1 M sodium formate. The photovoltammogram scans were obtained using a slow potential sweep (2 mV/s) in conjunction with interrupted irradiation (0.1 Hz) of the semiconductor film. All electrolyte solutions were sparged with ultrapure N_2 for at least 20 min prior to use. All measurements described below were performed at the laboratory ambient temperature (25 ± 2 °C).

Other Instrumentation. For scanning electron microscopy (SEM), a Zeiss Supra 55 instrument with a nominal electron beam voltage of 5 kV was used. Most of the films in this study were subjected to a thermal anneal in a model 650-14 Isotemp Programmable Muffle Furnace (Fisher Scientific) in air before characterization and photoelectrochemical measurements. A linear heat ramp (at 10 °C/min) from room temperature to a preselected final temperature of 450 °C was followed by a 30 min equilibration at the final temperature. The samples were then allowed to cool via natural convection in the furnace back to the ambient condition. X-ray powder diffraction (XRD) patterns of the samples were obtained on a Siemens D-500 powder diffractometer using Cu Kα radiation.

Results and Discussion

Nanoporous TiO_2 Films on Titanium Substrates. Table 1 contains a summary of the anodization conditions (columns 2−4). Early work by other groups employed dichromate−HF,[15] H_2SO_4–HF[18] mixtures, or dilute HF-containing electrolytes[17] as the anodization medium. The influence of other species or electrolyte compositions on the chemical dissolution/nanopore formation rates, e.g., $NH_4F/(NH_4)_2SO_4$ or NaF/Na_2SO_4 mixtures,[24−26,28] citric acid,[31] phosphate species,[23] or even nonaqueous (acetic acid) media,[27] was subsequently probed. The use of viscosity modifiers such as glycerol in the above media was reported[22] to afford smooth nanotubes of TiO_2 by suppressing local concentration fluctuations and pH bursts during anodization. In the present work, we used 0.15 M NH_4F as the electrolyte for Ti anodization, and other than glycerol, the influence of added poly(ethylene glycol) or PEG 400 (entry no. 8, Table 1) and D-mannitol (entry no. 9, Table 1) was also studied.

Fluoride ions induce pitting of the nascent oxide layer on titanium by forming soluble fluoro complexes and are essential

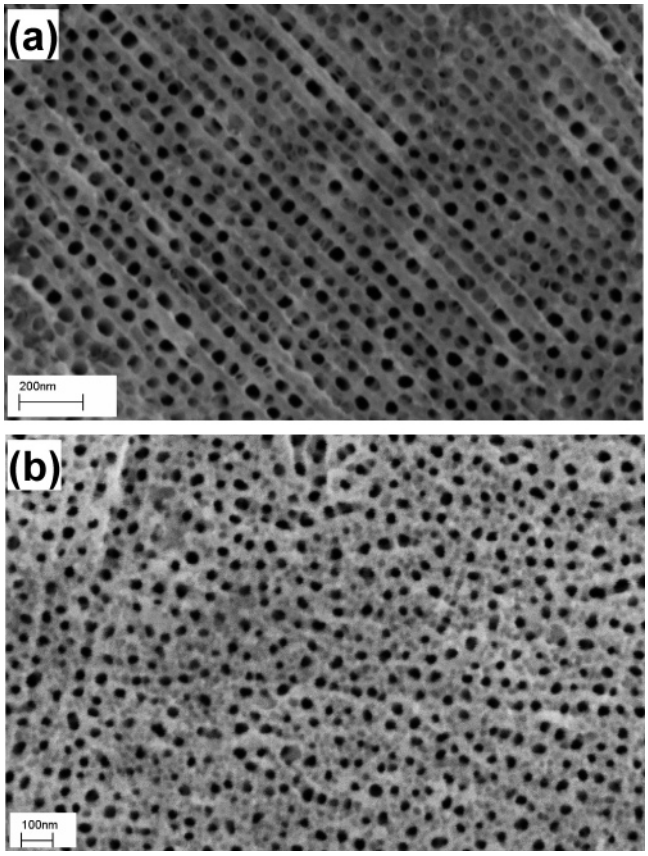

Figure 1. Effect of surface preparation on the morphology of TiO_2 films obtained by anodization at 20 V (5 h) in 0.15 M NH_4F/glycerol: (a) polished with sandpaper, 1200 grit, (b) mirror polished.

for nanopore formation. However, PEG is widely employed to modify interfacial behavior,[32] and D-mannitol (along with its derivatives) are known to form ligands with Ti to form soluble oligomers,[33] hence the choice of these two medium modifiers in the present work. Ammonium fluoride is soluble in glycerol under ultrasonication (entries 1−6, Table 1) but not in PEG 400 (entry 8, Table 1), and so a mixture of PEG ($HO-(CH_2-CH_2-O)_n-H$) and water was used to dissolve NH_4F in this case. An aqueous solution of D-mannitol ($HO-CH_2-(CH-OH)_4-CH_2-OH$) was similarly used in conjunction with NH_4F (entry 9, Table 1).

Figure 1 contains representative SEM pictures showing the influence of surface pretreatment (polish history) on the TiO_2 nanopore morphology. When the Ti foil is polished with sandpaper, not resulting in a mirror finish but in microscopic grooves on its surface, the nanotube openings appear aligned along the grooves (Figure 1a). Clearly, these grooves represent more active areas where the complexing reaction with F^- ions and oxide dissolution can occur. On the other hand, on a mirror-polished Ti foil the nanotubes appear as drilled channels distributed throughout the film (Figure 1b). Interestingly, if the Ti foil was not polished prior to anodization, nanotube formation was not facile. Presumably, the preexisting, native oxide skin is not conducive to nanopore formation on the Ti surface.

In general, the nanotube length increases with polarization time, and for an anodization voltage (time) of 40 V (10 h), TiO_2 nanotubes of 2.2 μm length were obtained. A representative SEM cross-section of these nanotubes is contained in Figure 2a. A lower anodization voltage (time) of 20 V (10 h) provided nanotubes 1.3 μm in length. Nanotubes up to 2.5 μm in length have been reported by other authors,[28] and even longer nanotube dimensions (up to 13 μm) have been attained by galvanostatic anodization.[34] Clearly, mass transport limitations do not adversely affect layer thickness if the anodization conditions are carefully tuned.[23,25,28] This contrasts with the situation for the anodic growth of *compact* semiconductor layers on metal substrates.[35]

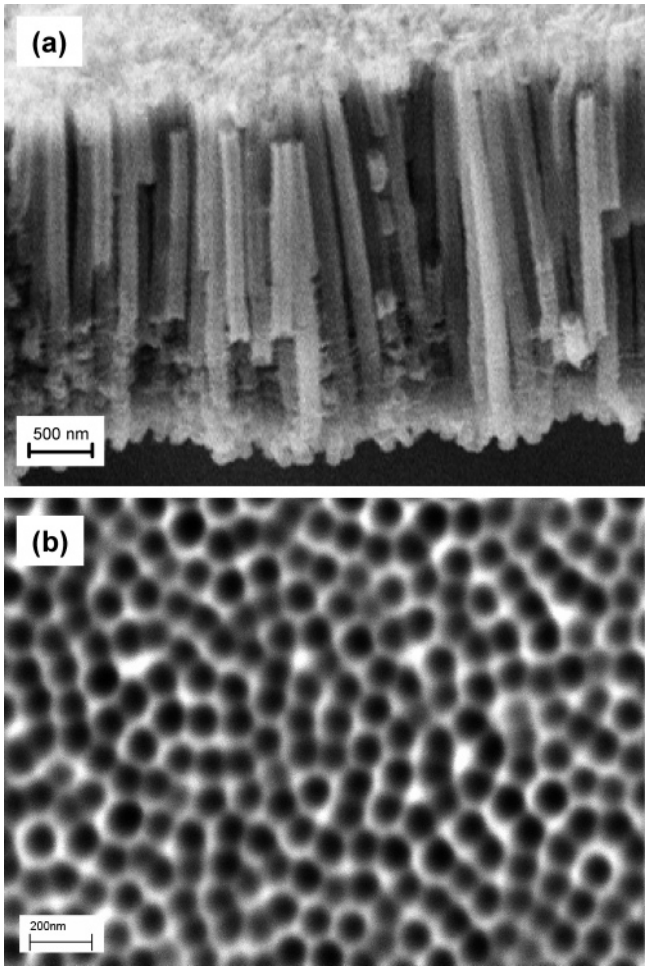

Figure 2. Scanning electron micrographs of a nanoporous TiO_2 film from anodization of Ti foil (40 V, 10 h) in 0.15 M NH_4F/glycerol: (a) cross-section and (b) footprint on the Ti substrate after peel-off of the nanoporous oxide layer. The peel-off was induced by bending the Ti/TiO_2 foil.

Anodization voltages ranging from 15 to 55 V were employed in the present study for TiO_2 (Table 1). Generally, voltages in the 20−40 V range resulted in uniform and self-organized nanotubes, while both lower and higher voltages resulted in disorganized nanoarchitectures. Nanotubes grown at 40 V for 10 h were very uniform and had a pore diameter of ∼90 nm (Figure 2). These nanotubes were both longer and wider than their counterparts at 20 V, reaching lengths up to ∼2.2 μm. Figure 3 contrasts the TiO_2 nanopore morphologies obtained (under otherwise comparable anodization conditions) for 0.15 M NH_4F in the presence of three medium modifiers: glycerol (Figure 3a), PEG 400 (Figure 3b), and D-mannitol (Figure 3c). The nanopores in glycerol were of the smallest diameter (40 nm), while PEG 400 and D-mannitol afforded nanotubes with diameters of 108 and 140 nm, respectively. Interestingly, while the nanotubes from glycerol-containing media had a drilled-in appearance (Figure 3a), those with PEG 400 and D-mannitol yielded TiO_2 nanotubes arranged in bundles with each pore having its own individual walls (Figure 3b and c). The nanotubes grown from D-mannitol-containing media even had multiple (up to three) compartments within them (Figure 3c).

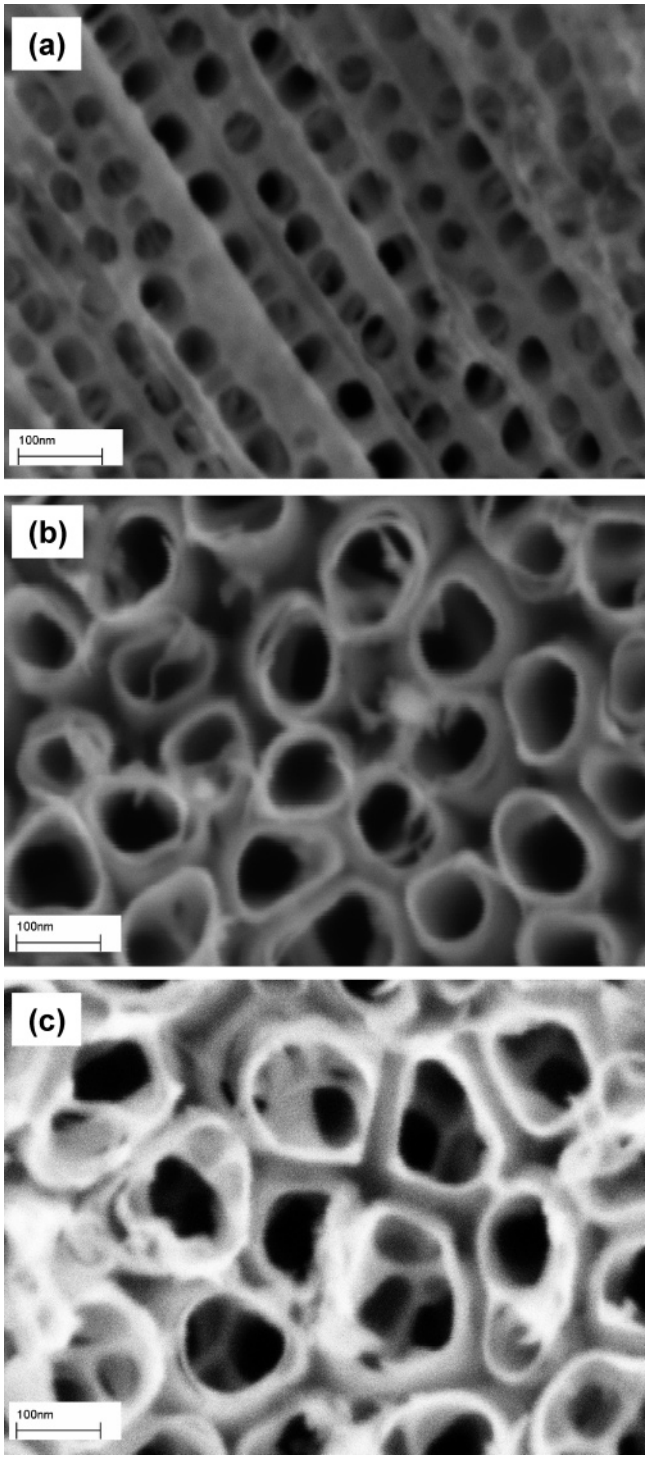

Figure 3. Comparison of SEM morphologies of nanoporous TiO_2 films obtained by anodization of Ti foil (20 V, 5 h) in 0.15 M NH_4F and (a) glycerol, (b) PEG 400, and (c) D-mannitol.

Consistent with the trends observed in previous studies,[24,26] as-grown TiO_2 layers were amorphous (XRD-silent) while the films subjected to thermal anneal showed the anatase structure. The mean grain size was estimated using the Scherrer formula[36] and found to be 12.76 nm (using the (105) peak). Again, in accord with previous findings, thermal anneal did not noticeably disrupt or alter the TiO_2 nanopore morphology.

The photoelectrochemical response of the nanoporous TiO_2 films was assessed using linear sweep photovoltammetry[4,8] in Na_2SO_4 supporting electrolyte with and without added formate species. As elaborated elsewhere,[37] photovoltammetry (a voltammetry experiment involving a slow potential ramp coupled with interrupted illumination of the semiconductor surface) permits evaluation of both the "dark" electrochemical behavior and the photoresponse of the film in one experiment and under identical experimental conditions. In the Na_2SO_4 electrolyte, the photogenerated holes in TiO_2 (that escape recombination) oxidize either adsorbed water molecules or hydroxyl groups, while the presence of formate furnishes a much more facile pathway for the transfer of holes across the film/electrolyte interface. Current-doubling processes (stemming from the initial generation of formate radicals followed by the injection of electrons from these radicals back into the oxide film, see below)[38] also occur in the latter cases. A figure-of-merit indicator of the quality of photoelectrochemical response is the steady-state photocurrent density, j_{ph}, measured in the plateau region of the photovoltammograms. Such values are contained in Table 1 (columns 5 and 6) for both the water and formate photooxidation cases.

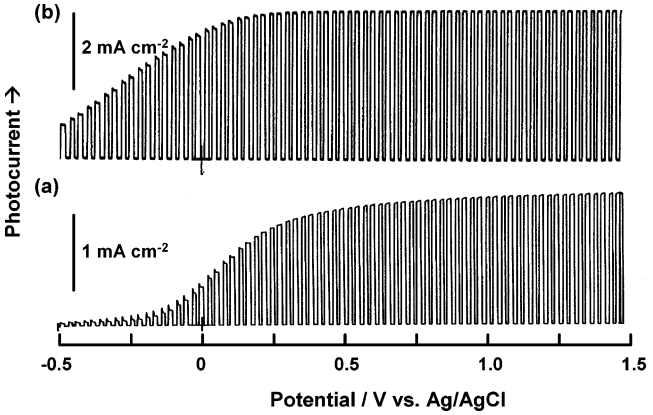

Figure 4. Linear-sweep photovoltammograms with 0.1 Hz chopped irradiation of a nanoporous TiO_2 film obtained by anodization of Ti foil (20 V, 10 h) in 0.15 M NH_4F/glycerol in (a) 0.5 M Na_2SO_4 supporting electrolyte and (b) 0.5 M Na_2SO_4 + 0.1 M HCOONa. Photovoltammograms were obtained at 2 mV/s using the full output of a 150 W Xe lamp.

Figure 4 shows photovoltammograms for a TiO_2 nanotube array by anodization at 20 V for 10 h (entry 3, Table 1). The higher photocurrent density (note the different current density scale in Figure 4a and b) and the photocurrent onset shift to negative potentials in the presence of formate are both consistent with the ability of formate to efficiently capture the photogenerated holes from TiO_2. The photoresponse is particularly good at this condition, and lower and higher anodization voltages result in inferior photoresponse as shown in Figure 5. These trends are consistent with the notion that any disorder in the nanopore film architecture has a deleterious influence on the photoelectrochemical response of the TiO_2 film. Presumably, O_2 or CO_2 gas (incipiently generated from water and formate photooxidation, respectively) remains trapped within the disorder architecture, thus impeding current flow.

Figure 6 contains another manifestation of the anodization voltage effect in terms of the photoresponse quality of the resultant film. Note that the film grown at 35 V shows a much more gradual attainment of the steady-state plateau response diagnostic of extensive carrier recombination (Figure 6b). On the other hand, films grown at 20 V show an abrupt rise in the photocurrent as the potential is swept past the flat-band situation (cf., Figures 4a and 6a).

It must be noted that the inferior photoresponse noted for the 15 V film in Figure 5 is *not* a consequence of the oxide film being too thin relative to the excitation light penetration

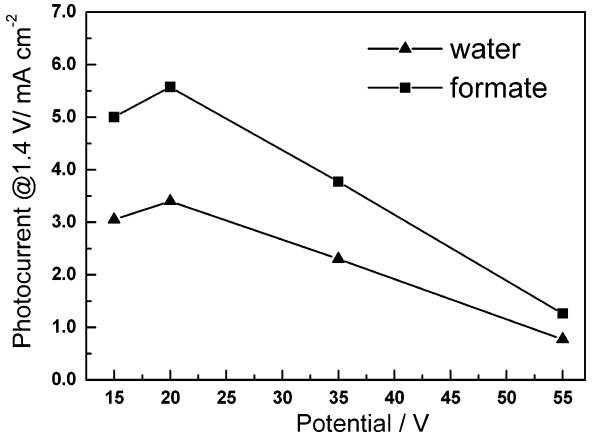

Figure 5. Effect of anodization voltage on the steady-state photocurrent density (j_{ph}). The j_{ph} values (also see Table 1) were culled from photovoltammograms as those in Figure 4.

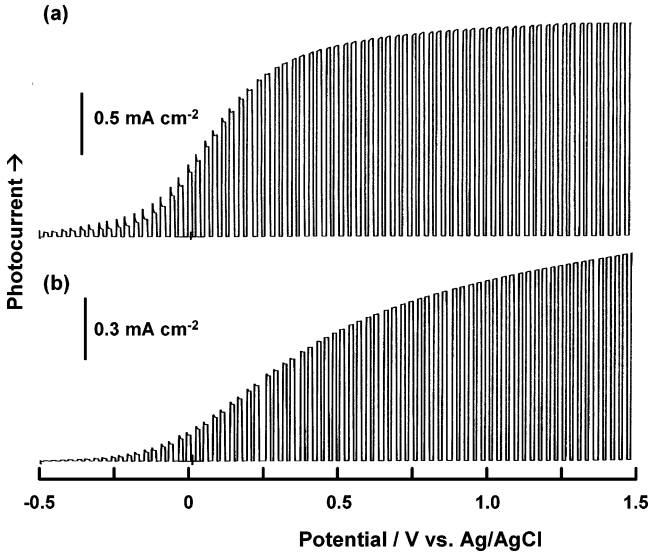

Figure 6. Linear-sweep photovoltammograms with 0.1 Hz chopped irradiation for nanoporous TiO_2 films obtained by anodization of Ti foil at (a) 20 and (b) 35 V. The anodization time in each case was 10 h, the medium was 0.15 M NH_4F/glycerol, and the photovoltammograms were acquired in 0.5 M Na_2SO_4. Other details are as in Figure 4.

depth (L_λ). In the cases considered here, the nanoporous layer dimension (thickness) is such that it is much higher than L_λ at all wavelengths relevant here. For example, L_λ is only 200 nm at $\lambda = 340$ nm, while the nanoporous layer is nominally micrometers thick.

Nanoporous WO_3 Films on Tungsten Substrates. Table 1 shows that an extensive set of conditions (relative to the TiO_2 case) were considered for the anodic growth of nanoporous WO_3. Oxalic acid[29] and NaF[30] electrolytes were used in two previous studies on this material. We additionally studied the effect of glycerol on the anodic growth of WO_3 in the oxalic acid electrolyte (entries 19−22, Table 1).

Figure 7 illustrates the effect of anodization time at constant voltage on film morphology, while Figure 8 shows the effect of anodization voltage. At low process times, the nanopore structure is not fully developed on the entire surface (Figure 7a) as it is after 1 h at 35 V (Figure 7b). At longer times (e.g., 5 h) the pore organization is disrupted and the morphology changes to a disordered appearance (Figure 7c). Low voltages, e.g., 10 V (Figure 8a), give rise to nanocube clusters, while intermediate voltages (e.g., 35 V) generate WO_3 surfaces with

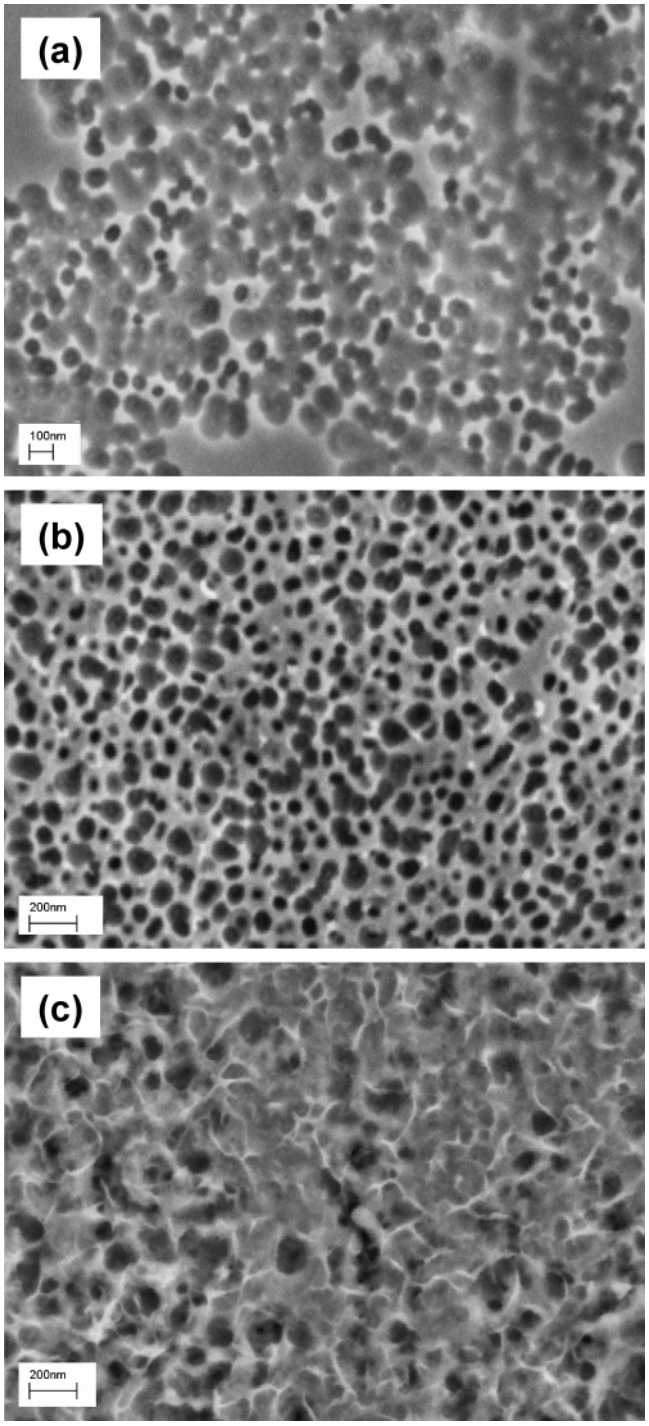

Figure 7. Effect of anodization time on the morphology of nanoporous WO_3 films as probed by SEM. The films were grown in 0.3 M oxalic acid medium at 35 V for (a) 30, (b) 60, and (c) 300 min.

an array of bowl-shaped nanostructures (Figure 8b). High anodization voltages (e.g., 60 V) give rise to collapsed nanowires with a tepee-like appearance (Figure 8c).

The effect of glycerol addition to the oxalic acid electrolyte was investigated. The anodization voltage was kept constant in this set of experiments, while the ratio of glycerol to water was changed. As the ratio increases, the number of nanobowl-like features systematically decreased, and with a 90:10 (glycerol: water) ratio, the resultant WO_3 film was of dark blue hue and compact (entries 19−21, Table 1). Higher voltages (e.g., 55 V) at this composition yielded a very uniform smooth film (entry 22, Table 1).

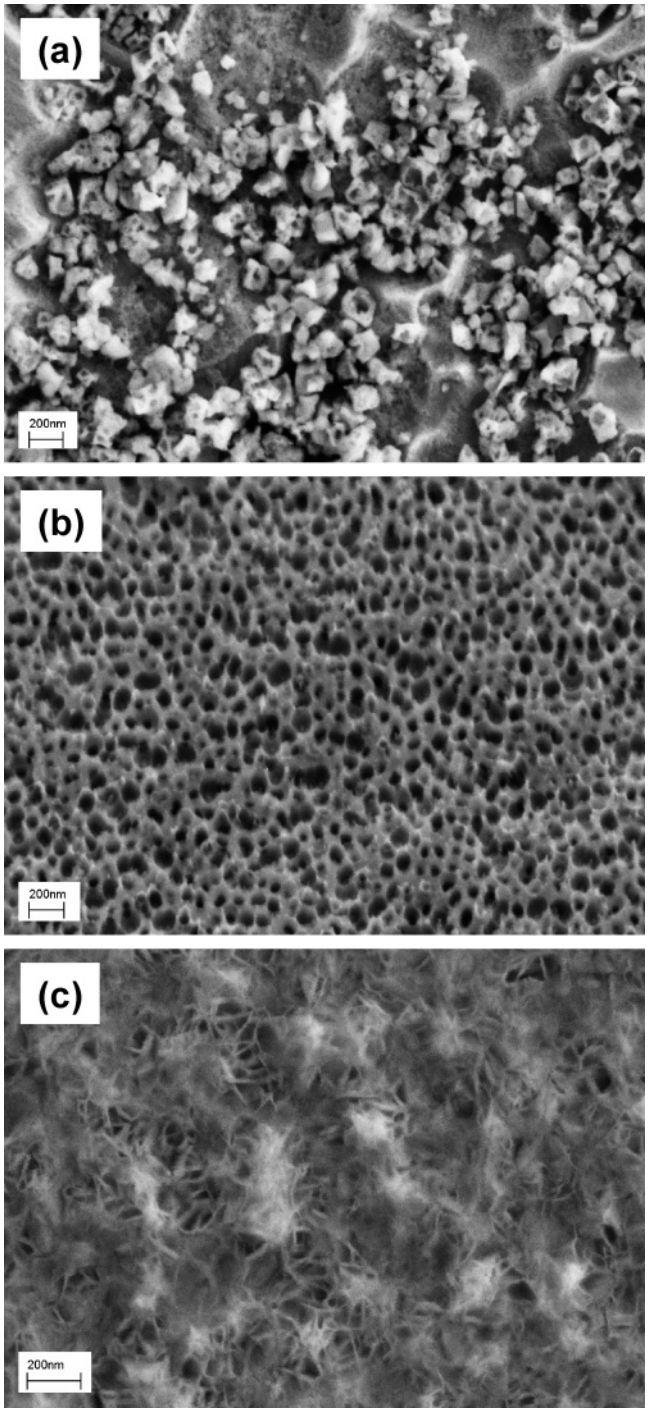

Figure 8. As in Figure 7 but showing the effect of anodization voltage. The anodization medium was 0.3 M oxalic acid, the anodization time was 1 h, and the voltage was (a) 10, (b) 35, and (c) 55 V.

Films were also grown in NaF electrolytes (as in previous studies), and representative micrographs are contained in Figures 9 and 10b. Dark blue films were obtained in these cases, but the porous films were much more disordered relative to the examples in Figures 7b and 8b. The effect of thermal anneal is illustrated in Figure 9b and c. Unlike in the TiO_2 cases discussed earlier, the WO_3 film morphology indeed is influenced by the anneal treatment and is significantly more crystalline (see below). Addition of HF to the NaF electrolyte (entry 26, Table 1) does affect the film morphology and nanoporous structure (cf., Figure 10b and c). Figure 10 provides a SEM comparison of the WO_3 films obtained in the three electrolytes under otherwise identical anodization conditions.

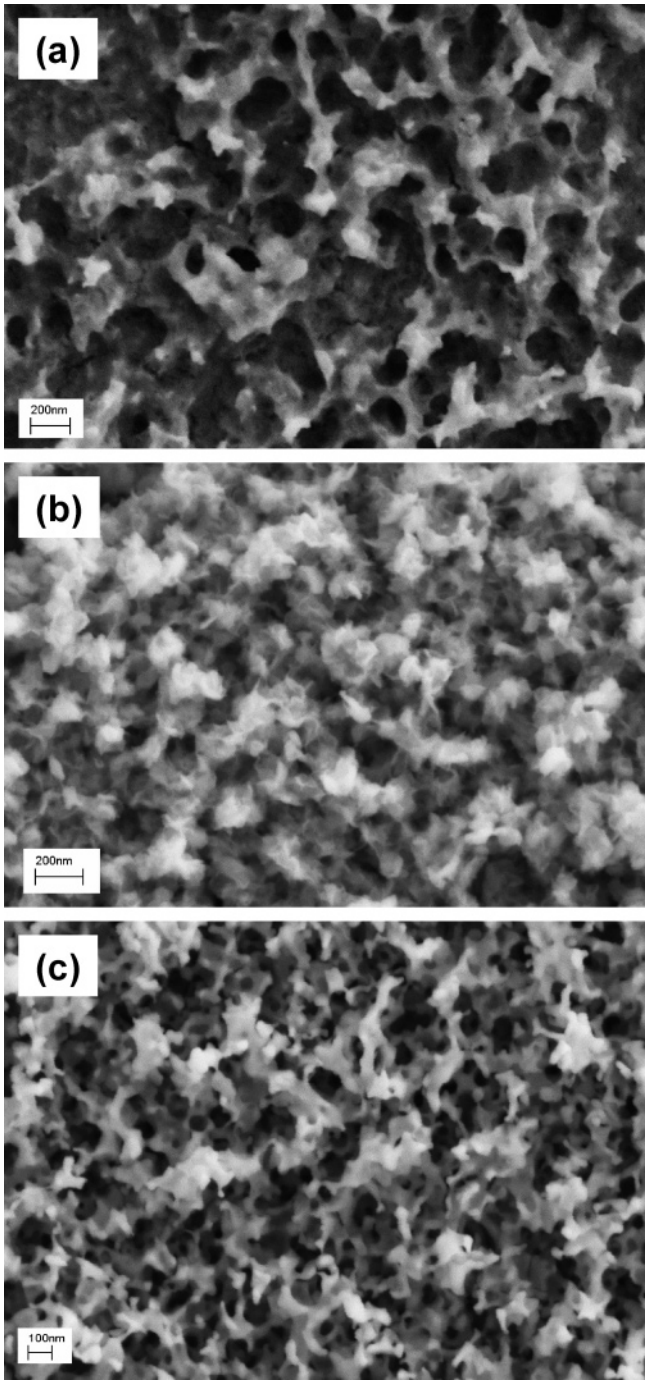

Figure 9. Morphology of nanoporous WO_3 films obtained by anodization of W foil (60 V) in 0.15 M NaF electrolyte. The anodization time was 1 and 3 h in Figure 9a and b, respectively. Growth conditions in Figure 9c are same as those in Figure 9b except that the as-grown film was subjected to thermal anneal.

As with TiO_2, the as-deposited WO_3 films were amorphous in all cases. After thermal anneal, the films reverted to a monoclinic structure as seen by XRD.[29] The mean grain size was estimated using the Scherrer formula and found to be 32.37 nm (with the (160) peak).

Selected photovoltammograms for anodic WO_3 films are contained in Figures 11−13. Particularly high-quality photoresponses are shown by the films considered in Figures 11b and 12c (corresponding to entries 15 and 24, Table 1). As with TiO_2, both low and high anodization voltages are deleterious in terms of photoresponse quality (Figure 11). Similarly, low and high anodization times are not optimal (cf., Figure 12a, c, d). Addition

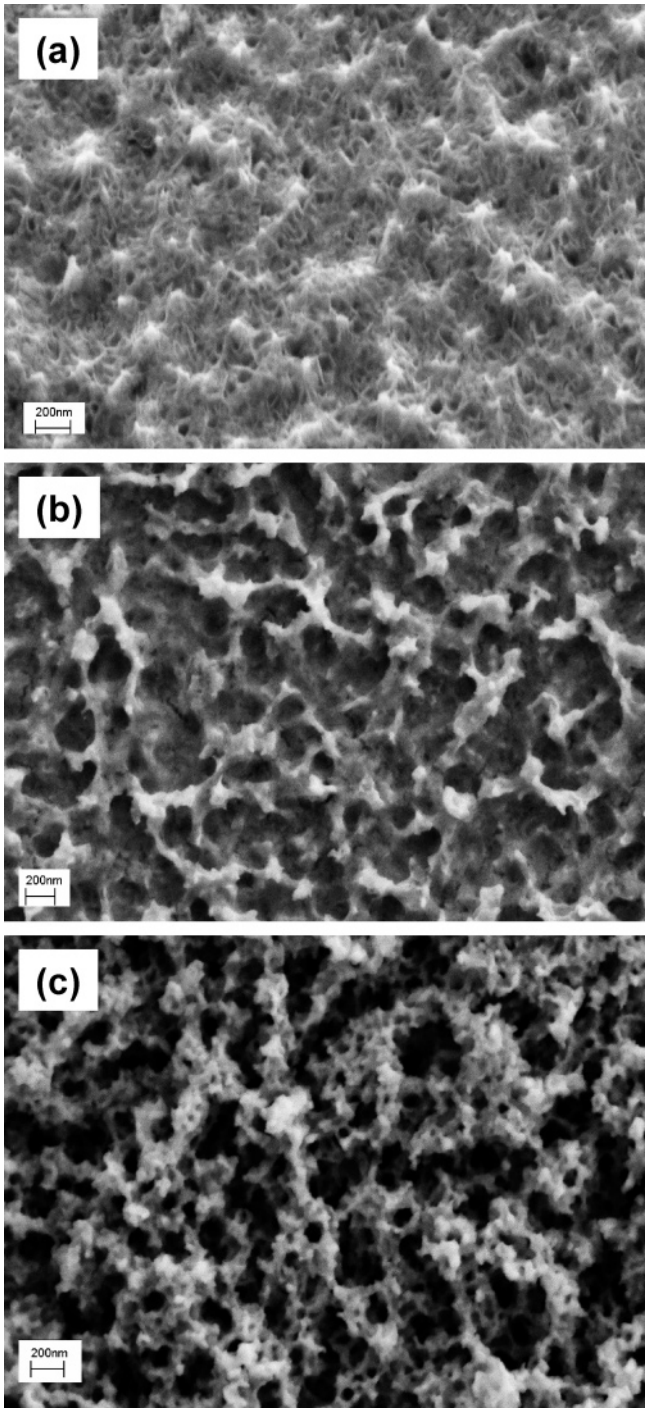

Figure 10. Comparison of SEM film morphology for nanoporous WO_3 films obtained by anodization of W foil (60 V, 1 h) in (a) 0.3 M oxalic acid, (b) 0.15 M NaF, and (c) 0.15 M NaF + 0.05 M HF aqueous electrolytes.

of HF to the NaF electrolyte does not appear to exert a marked influence on the photoresponse (cf., Figure 12a and b). Interestingly, the films obtained at low anodization voltages yield a twin-plateau photovoltammogram profile (Figure 11a) diagnostic of the water oxidation reaction passing through a peroxide intermediate stage. Finally, as with the TiO_2 cases discussed earlier, addition of formate to the Na_2SO_4 supporting electrolyte exerts a marked enhancement of the photoelectrochemical response as shown by the examples in Figure 13 (also see columns 5 and 6 for entries 19−26, Table 1). The factors underlying this enhancement were discussed earlier.

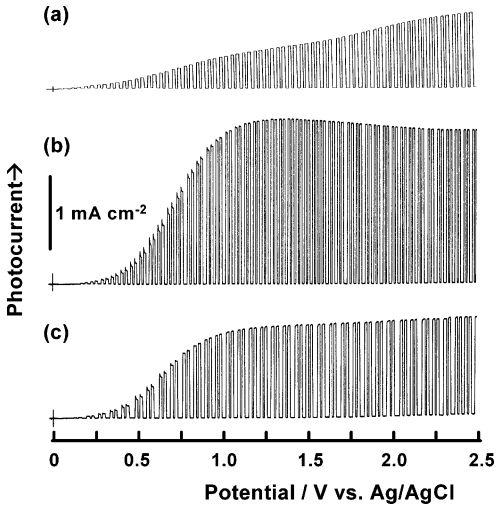

Figure 11. Linear-sweep photovoltammograms with 0.1 Hz chopped irradiation for nanoporous WO_3 films in 0.5 M Na_2SO_4. The films were obtained by anodization of W foil in 0.3 M oxalic acid: (a) 10 V, 30 min, (b) 35 V, 1 h, and (c) 55 V, 1 h. Photovoltammograms were obtained at 2 mV/s using the full output of a 150 W Xe lamp.

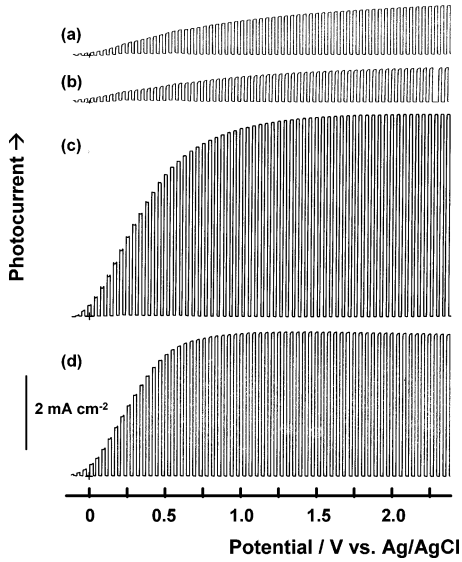

Figure 12. Linear-sweep photovoltammograms with 0.1 Hz chopped irradiation for nanoporous WO_3 films in 0.5 M Na_2SO_4 + 0.1 M HCOONa. These films were formed by anodization in 0.15 M NaF at 60 V for (a) 1, (c) 3, and (d) 6 h. The scan in Figure 12b pertains to a film grown in 0.15 M NaF + 0.05 M HF under conditions similar to those in Figure 12a. Other details are as in Figure 11.

As in the case of TiO_2, the nanoporous layer thickness is not a limiting factor in dictating the magnitude of the photocurrents measured for the WO_3 samples.

Comparative Aspects for TiO_2 and WO_3. Figure 14 provides a telling comparison of the nanopore morphology of the two oxide semiconductors films obtained under identical anodization conditions, namely, 20 V for 10 h in 0.15 M NH_4F/glycerol. The nanopore formation clearly is less facile and ordered in WO_3 (Figure 14b) relative to TiO_2 (Figure 14a). The average nanotube diameter was ca. 40 and 13 nm for TiO_2 and WO_3, respectively. Clearly, the differing ability of Ti and W to undergo the twin (and finely balanced) processes of oxide formation and dissolution in the F^- ion-containing electrolyte plays a crucial role in the proclivity to self-organized nanopore formation.

Photoaction spectra for TiO_2 and WO_3 films in 0.5 M Na_2SO_4 + 0.1 M HCOONa are compared in Figure 15 where

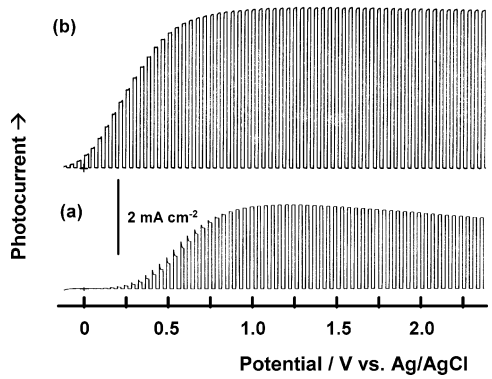

Figure 13. As in Figure 12 but showing the influence of formate addition. The film was obtained by anodization of W foil at 60 V (6 h) in 0.15 M NaF. The photovoltammograms were obtained in (a) 0.5 M Na_2SO_4 and (b) 0.5 M Na_2SO_4 + 0.1 M HCOONa.

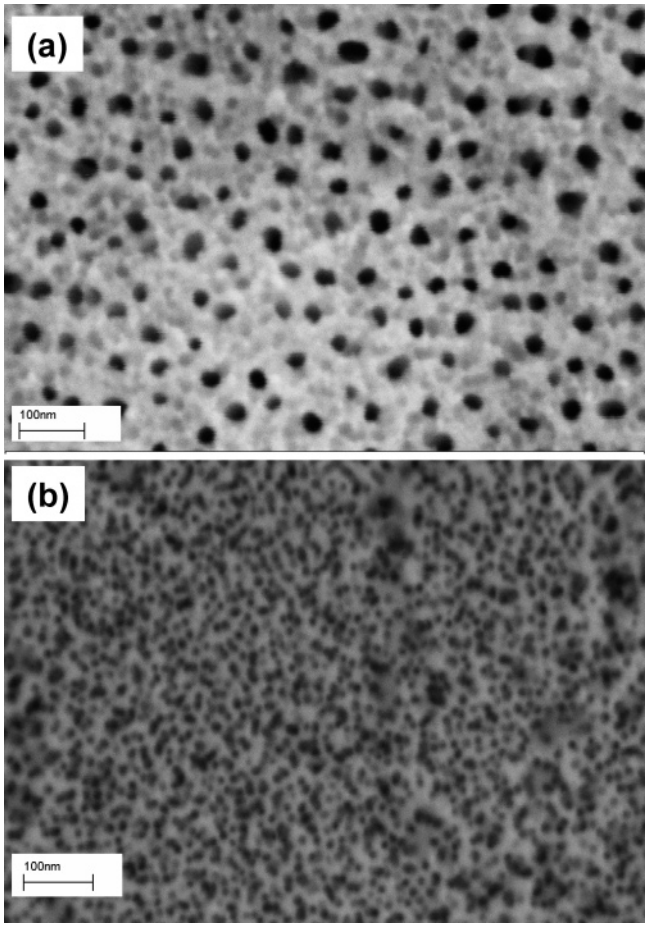

Figure 14. Comparison of morphologies of TiO_2 (Figure 14a) and WO_3 (Figure 14b) nanoporous films as probed by SEM. Both films were grown at 20 V (10 h) in 0.15 M NH_4F/glycerol.

the incident photon to electron conversion efficiency (IPCE) is plotted vs wavelength for various preparation protocols

$$\mathrm{IPCE} = (i_{ph}/q\varphi) \times 100$$

where i_{ph} is the photocurrent density, q is the electronic charge, and φ is the incident photon flux density at the photoelectrode location. The following trends are worth noting. (a) Excellent performance is observed for the two oxide semiconductor films with IPCE values in the range 130−190% for TiO_2 and 120−180% for WO_3; these values depend on the preparation procedure. (b) The spectral response is more extended to the visible region for WO_3 than for TiO_2. (c) Best performance is obtained for films prepared from NH_4F in PEG 400 for TiO_2 and from aqueous NaF solutions for WO_3, although very high IPCE values were also obtained for both oxide semiconductor films prepared from NH_4F in glycerol.

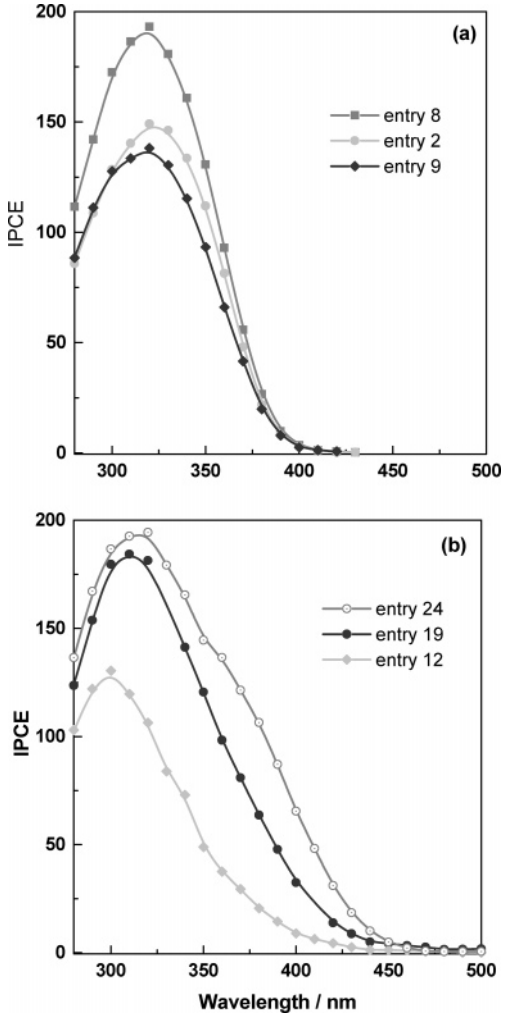

Figure 15. Photoaction spectra (IPCE vs wavelength) of nanoporous TiO_2 and WO_3 films in 0.5 M Na_2SO_4 + 0.1 M HCOONa. The stationary photocurrent density was measured monochromatically at 1.5 and 2.0 V for TiO_2 and WO_3, respectively. Figure 15a compares spectra for TiO_2 films prepared with NH_4F in PEG 400, glycerol, and D-mannitol (entries 8, 2, and 9 in Table 1). Figure 15b compares spectra for WO_3 films prepared with aqueous NaF with those from oxalic acid in glycerol:water (25:75) mixtures and with NH_4F in glycerol (entries 24, 19, and 12 in Table 1).

IPCE values higher than 100% are consistent with the "current-doubling" effect of the formate additive.[38] When organic species R^- (R = HCOO, CH_3COO) are present in the electrolyte, the one-electron oxidation reaction ($R^- + h^+ \rightarrow R^\bullet$) proceeds with facile kinetics and the current-doubling phenomenon arises from the fact that the radical intermediate $R^\bullet$ can inject an electron into the semiconductor conduction band ($R^\bullet \rightarrow R^+ + e^-$) promoting a doubling of the anodic photocurrent value (see above).

A comparison of our nanoporous WO_3 films with those very recently reported by other authors[39] and also with films obtained by us by cathodic electrodeposition[40] is quite illuminating. IPCE values of ca. 30% were reported in the absence of an electron donor for nanoporous WO_3 prepared from 1 M H_2SO_4 + 0.5 wt % NaF for 1 h at 40 V vs Ag|AgCl,[39] while we obtained

IPCE values near 20% under similar experimental conditions for the cathodically formed WO_3 (see ref 40, Figure 5a).

Concluding Remarks

The present study builds upon the literature on nanoporous TiO_2[15−28] and WO_3[29,30,39] films obtained by anodization of Ti and W substrates in corrosive media. Self-organized TiO_2 nanotubes grown in the presence of glycerol, PEG 400, and D-mannitol afforded nanopores with diameters of 40, 108, and 140 nm respectively. This self-organized nanopore morphology is shown to yield an excellent quality of photoelectrochemical response using the photooxidation of water and organic species as reaction probes. For example, the dark (leakage) currents in these films were negligible, attesting to the excellent rectification property of the resultant semiconductor/electrolyte contacts. Reverse bias potentials up to ∼1.5 V for TiO_2 and ∼2.5 V for WO_3 were applied without any evidence of anodic film break down (from carrier tunneling processes, etc). The photocurrent densities for the nanoporous TiO_2 and WO_3 films were significantly higher (by orders of magnitude) than those obtained with the corresponding compact film counterparts (obtained, for example, by cathodic electrodeposition, cf., refs 40 and 41), attesting to the usefulness of these nanoarchitectures for solar energy conversion applications (also see refs 19, 20, and 24). The correlation between nanopore morphology and photoelectrochemical behavior, however, is complex. While nanopore order and self-organization are clearly important factors, anodization conditions affording other morphologies do yield respectable photoresponse quality in some instances, and this is especially true for the WO_3 samples considered in this study. Further work will be aimed at unraveling the mechanistic aspects of nanopore growth and the use of nanoporous structures for solar energy conversion applications.

Acknowledgment. This article was dedicated to Art Nozik in honor of his extensive and sustained contributions to the field of semiconductor photoelectrochemistry and solar energy conversion over a period spanning three decades. This work was supported in part by a grant from the U.S. Department of Energy (Office of Basic Energy Sciences). We thank Eugenio Tacconi for the kind donation of the multioutput power supply. We thank the three anonymous reviewers for their constructive criticism of an earlier manuscript version.

References and Notes

(1) Nozik, A. J.; Memming, R. *J. Phys. Chem.* **1996**, *100*, 13061.
(2) Lewis, N. S. *J. Phys. Chem.* **1998**, *102*, 4843.
(3) Lewis, N. S. *J. Electroanal. Chem.* **2001**, *508*, 1.
(4) Rajeshwar, K. In *Encyclopedia of Electrochemistry: Semiconductor Electrodes and Photoelectrochemistry*; Licht, S., Ed.; Wiley-VCH: Weinheim, Germany, 2002; Vol. 6, Chapter 1, pp 1−53. See also other chapters in this volume.
(5) Hodes, G.; Howell, I. D. J.; Peter, L. M. *J. Electrochem. Soc.* **1992**, *139*, 3136.
(6) Hagfeldt, A.; Grätzel, M. *Chem. Rev.* **1995**, *95*, 49.
(7) Santato, C.; Ulmann, M.; Augustynski, J. *J. Phys. Chem. B* **2001**, *105*, 936.
(8) Zhou, M.; Lin, W.-Y.; de Tacconi, N. R.; Rajeshwar, K. *J. Electroanal. Chem.* **1996**, *402*, 221.
(9) Masuda, H.; Fukuda, K. *Science* **1995**, *268*, 1466.
(10) Masuda, H.; Fukuda, K. *Appl. Phys. Lett.* **1997**, *71*, 2770.
(11) Masuda, H.; Hasegwa, F.; Ono, S. *J. Electrochem. Soc.* **1997**, *144*, L127.
(12) Jessensky, O.; Muller, F.; Gösele, U. *Appl. Phys. Lett.* **1998**, *72*, 1173.
(13) Canham, L. T. *Appl. Phys. Lett.* **1990**, *57*, 1046.
(14) Lehmann, V.; Gösele, U. *Adv. Mater.* **1992**, *4*, 116.
(15) Zwilling, V.; Aucouturier, M.; Darque-Ceretti, E. *Electrochim. Acta* **1999**, *45*, 921.
(16) Gong, D.; Grimes, C. A.; Varghese, O. K.; Hu, W.; Singh, R. S.; Chen, Z.; Dickey, E. C. *J. Mater. Res.* **2001**, *16*, 3331.
(17) Mor, G. K.; Varghese, O. K.; Paulose, M.; Mukherjee, N.; Grimes, C. A. *J. Mater. Res.* **2003**, *18*, 2588.
(18) Beranek, R.; Hildebrand, H.; Schmuki, P. *Electrochem. Solid-State Lett.* **2003**, *6*, B12.
(19) Mor, G. K.; Shankar, K.; Paulose, M.; Varghese, O. K.; Grimes, C. A. *Nano Lett.* **2005**, *5*, 191.
(20) Varghese, O. K.; Paulose, M.; Shankar, K.; Mor, G. K.; Grimes, C. A. *J. Nanosci. Nanotechnol.* **2005**, *5*, 1158.
(21) Ruan, C.; Paulose, M.; Varghese, O. K.; Mor, G. K.; Grimes, C. A. *J. Phys. Chem.* **2005**, *109*, 15754.
(22) Macak, J. M.; Tsuchiya, H.; Taveira, L.; Aldabergerova, S.; Schmuki, P. *Angew. Chem., Int. Ed.* **2005**, *44*, 7463.
(23) Ghicov, A.; Tsuchiya, H.; Macak, J. M.; Schmuki, P. *Electrochem. Commun.* **2005**, *7*, 505.
(24) Beranek, R.; Tsuchiya, H.; Sugishima, T.; Macak, J. M.; Taveira, L.; Fujimoto, S.; Kisch, H.; Schmuki, P. *Appl. Phys. Lett.* **2005**, *87*, 243114.
(25) Macak, J. M.; Sirotna, K.; Schmuki, P. *Electrochim. Acta* **2005**, *50*, 3679.
(26) Tsuchiya, H.; Macak, J. M.; Ghicov, A.; Taveira, L.; Schmuki, P. *Corros. Sci.* **2005**, *47*, 3324.
(27) Tsuchiya, H.; Macak, J. M.; Taveira, L.; Balaur, E.; Ghicov, A.; Sirotna, K.; Schmuki, P. *Electrochem. Commun.* **2005**, *7*, 576.
(28) Macak, J. M.; Tsuchiya, H.; Schmuki, P. *Angew. Chem., Int. Ed.* **2005**, *44*, 2100.
(29) Mukherjee, N.; Paulose, M.; Varghese, O. K.; Mor, G. K.; Grimes, C. A. *J. Mater. Res.* **2003**, *18*, 2296.
(30) Tsuchiya, H.; Macak, J. M.; Sieber, I.; Taveira, L.; Ghicov, A.; Sirotna, K.; Schmuki, P. *Electrochem. Commun.* **2005**, *7*, 295.
(31) Cai, Q.; Paulose, M.; Varghese, O. K.; Grimes, C. A. *J. Mater. Chem.* **2005**, *20*, 230.
(32) In *Poly(ethylene Glycol): Chemistry and Biological Applications*; Harris, J. M., Zalipsky, S., Eds.; American Chemical Society, Washington, DC, 1997.
(33) Hegarty, P.; Lau, R.; Motherwell, W. B. *Tetrahedron Lett.* **2003**, *44*, 1851.
(34) Grimes, C. A. Personal communication, June 2006.
(35) Ham, D.; Mishra, K. K.; Rajeshwar, K. *J. Electrochem. Soc.* **1991**, *138*, 100 and references therein.
(36) Cullity, B. D. *Elements of X-Ray Diffraction*; Addison-Wesley: Reading, MA, 1967.
(37) Chenthamarakshan, C. R.; de Tacconi, N. R.; Shiratsuchi, R.; Rajeshwar, K. *J. Electroanal. Chem.* **2003**, *553*, 77.
(38) Morrison, S. R. *The Chemical Physics of Surfaces*; Plenum: New York, 1977.
(39) Berger, S.; Tsuchiya, H.; Ghicov, A.; Schmuki, P. *Appl. Phys. Lett.* **2006**, *88*, 203119.
(40) de Tacconi, N. R.; Chenthamarakshan, C. R.; Rajeshwar, K.; Pauporté, T.; Lincot, D. *Electrochem. Commun.* **2003**, *5*, 220.
(41) Somasundaram, S.; Tacconi, N.; Chenthamarakshan, C. R.; Rajeshwar, K.; de Tacconi, N. R. *J. Electroanal. Chem.* **2005**, *577*, 167.